Journal of Environmental Chemical Engineering 5 (2017) 310–318

Contents lists available at ScienceDirect

Journal of Environmental Chemical Engineering

journal homepage: www.elsevier.com/locate/jece

Cu-decorated Raschig-TiO_2 rings inducing MB repetitive discoloration without release of Cu-ions under solar light

Laura Suárez[a], Zhang Wei[a,b], Helena Teixidó[a], Rosendo Sanjinés[c], Michaël Bensimon[d], César Pulgarín[a,*], John Kiwi[a,*]

[a] Ecole Polytechnique Fédérale de Lausanne, EPFL-SB-ISIC-GPAO, Station 6, CH-1015, Lausanne, Switzerland
[b] Tongji University, 1239 Siping Rd, Yangpu, Shanghai, China
[c] Ecole Polytechnique Fédérale de Lausanne, EPFL-SB-IPMC-LNNME, Bat PH, Station 3, CH-1015, Lausanne, Switzerland
[d] Ecole Polytechnique Fédérale de Lausanne, EPFL-ENAC-IIEGR-CEL, Bat GC, Station 18, CH-1015 Lausanne, Switzerland

ARTICLE INFO

Article history:
Received 12 August 2016
Received in revised form 23 November 2016
Accepted 4 December 2016
Available online 5 December 2016

Keywords:
MB-discoloration
Sunlight
Light intensity effect
Mechanism
Intra-gap states
Roughness (Rg)

ABSTRACT

The methylene blue (MB) discoloration on innovative photocatalysts made up of Raschig-rings coated by pre-formed TiO_2 nanoparticles decorated with CuOx (RR@TiO_2-Cu) is presented. The MB-discoloration was drastically accelerated by the subsequent addition of 0.004% Cu. This Cu-content being ~3000 times below the TiO_2 present in the RR@TiO_2 samples led to MB-discoloration in shorter times. The Cu-ions released from the RR@TiO_2-Cu 0.004% were determined ≤1ppb by inductively coupled plasma mass-spectrometry (ICP-MS). Cu-percentages >0.018% decreased the MB-discoloration kinetics due to the Cu acting as recombination sites for the photogenerated charges. The total organic carbon (TOC) reduction concomitant with the MB-discoloration is reported as well as the effect of the initial MB-concentration and pH on the discoloration kinetics. The Cu-addition shifted significantly the TiO_2 absorption into the visible region even when added in sub-microgram quantities (0.004%) to RR@TiO_2 as detected by diffuse reflectance spectroscopy (DRS). The Cu level added to RR@TiO_2 was too low to be detected by X-ray diffraction (XRD). The roughness of the RR@TiO_2-Cu (0.018%–0.081% Cu) presented Rg-values between 11.8 nm and 23.9 nm. The RR@TiO_2Cu presented agglomerate sizes of ~200 nm for TiO_2 and for the Cu aggregates sizes of ~20 nm. The MB discoloration kinetics and reuse of the RR@TiO_2-Cu suggest the potential as a supported catalyst in environmental cleaning process. A reaction mechanism is suggested taking into consideration the role of the $Cu^{1+/2+}$ intra-gap states involving redox catalysis as detected by X-ray photoelectron-spectroscopy (XPS).

1. Introduction

TiO_2, doped TiO_2 and decorated TiO_2 either in colloid form or powder have been reported to degrade pollutants under band gap irradiation. Some studies report TiO_2 on glass/polymer and metal plates leading to pollutants. This subject has been the focus of recent reviews [1–6]. This type of catalysis/photocatalysis is used to degrade pollutants resistant to biological degradation at low concentrations involving reactions driven by solar light. In this case, the source of energy is free but its utilization requires facilities that involve capital investment. The reactions when light reaches the semiconductor surface (TiO_2) in the presence of O_2 (air) leads to the generation of charges and radicals not needing any additional reactant to abate the organic pollutant. In this study, we have selected as a probe the dye methylene blue (MB). Glass in the form of Raschig rings, was used as a low cost inert support for the TiO_2. TiO_2 coated Raschig rings have been used for the degradation of pollutants in diluted solutions under band-gap irradiation to abate the dye direct-red 16 [7]. This approach has also been used to degrade several aromatic compounds in aqueous solution [8–10]. Our laboratory has reported Raschig rings coated by TiO_2 as a catalyst to degrade phenol-compounds [11], phenol [12] and chlorophenols [13]. This study addresses the preparation of Raschig rings coated with TiO_2 but adding small amounts of a 3d-transition element like Cu/Cu-ions to extend its absorption into

* Corresponding authors.
E-mail addresses: cesar.pulgarin@epfl.ch (C. Pulgarín), john.kiwi@epfl.ch (J. Kiwi).

http://dx.doi.org/10.1016/j.jece.2016.12.006
2213-3437/

the visible region with the objective of increasing the dye degradation kinetics under solar light.

We address the simple preparation of a low-cost RR@TiO_2-Cu photocatalyst and its testing with the degradation of MB. Supported TiO_2 avoids the separation of the catalyst from the solution at the end of the dye degradation process. The degradation kinetics of Cu-decorated TiO_2 Raschig rings, the reaction mechanism, the Cu-ions leaching from the catalyst surface and the characterization of the optimized photocatalyst surface will be systematically investigated in the course of this study.

2. Materials and methods

2.1. Materials and synthesis of RR@TiO_2-Cu, reactor set-up, MB-discoloration, total organic carbon (TOC), X-ray fluorescence (XRF) and irradiation source

The Raschig rings that served as support for the RR@TiO_2-Cu were 4 × 4 mm in size and 1 mm thick, were made out of soda lime glass composed by: 70% SiO_2, 10% (Na_2O, CaO, MgO K_2O) and 5% (Fe_2O_3, $Al2O_3$). TiO_2 used in the suspensions was Degussa P25 and the $CuNO_3 \times 3H_2O$ was Acros Organics. The polyethylene-graft-maleic anhydride powder (PEGMA) was a Sigma–Aldrich No.456624, Mw 2300. The reagent 3, 7-bis (Dimethylamino) phenazathionium chloride or Methylene Blue (MB from now) was Sigma-Aldrich and used as received. NaN_3 (Fluka) was used as a possible oxygen singlet scavenger ($^1O_2$). 1, 4-benzoquinone (BQ) and methanol were used respectively as $O_2^{\bullet -}$ radical scavenger and $OH^{\bullet}$ scavengers [14]. Ethylenediamine tetra-acetic acid (EDTA-2Na) was used as TiO_2vb hole scavenger [15].

The supported catalyst preparation was prepared according to the following sequence: the Raschig rings were washed with detergent and then treated with HNO_3 30% for 10 min at 50 °C, then drained and rinsed with Milli-Q water. The clean Raschig rings were subsequently immersed in PEGMA dissolved in toluene 5% (wt/wt), then drained and dried overnight at room temperature. The dry Raschig rings with PEGMA on their surface were dipped in TiO_2 suspensions (5 g/l) and $CuNO_3{\cdot}3H_2O$ was added according to the amount selected to decorate the RR@TiO_2. The rings were drained and dried at 110 °C for 1 h. The latter step was repeated 3 times and the RR@TiO_2-Cu was calcined at 500 °C during 10 h to eliminate the PEGMA, the interfacial binder. TiO_2/Cu was deposited on the external and internal surfaces of the Raschig rings. The reproducibility of the amount of Cu deposited on the RR@TiO_2 was ± 20% and it was kept by following the preparation protocol.

The UV–vis spectra during MB discoloration were followed in a Schimadzu single beam instrument. The total organic carbon (TOC) was determined in a Shimadzu TOC 500 equipped with an ASI auto-sampler. The Ti and Cu content in (RR@TiO_2-Cu) was evaluated by X-ray fluorescence in a PANalytical PW 2400 unit. The TiO_2 and Cu weight percentages on the RR@TiO_2 rings are reported in Table 1 and were determined by X-ray fluorescence spectroscopy. By this technique, each element emits a defined X-ray wavelength that is associated with the particular atomic number of each element. The different TiO_2-Cu suspensions used to prepare the rings were 0.05% up to 3% w/w Cu/TiO_2.

Photolysis experiments were performed in the cavity of a solar simulated Hanau Suntest Lamp with a tunable light intensity attachment equipped with an IR filter to remove IR radiation >800 nm. The UV-radiation <305 nm was removed by the Pyrex wall of the reaction vessels. The Raschig rings used to fix the TiO_2-Cu were positioned between a central Teflon cylindrical tube and the reactor wall; in this way the photocatalytic bed was fixed inside the reactor. The Teflon support was fitted with small holes (2 mm diameter) to allow diffusion of the solution in the reactor. In the bottom of the reactor, and concentrically to both the Teflon tube and the reactor, a magnetic stirrer was positioned to keep the diffusion of the reactive species. The Suntest solar simulator (Heraeus, Hannau, Germany) is shown in Fig. 1a. The reactors cavity was ~ 30 cm wide, 20 cm long and 20 cm high. The distance between the Xe-lamp and the photo-reactor lid was 10 cm. The photo-reactor was 7 cm high without the lid and 11 cm high with the lid. Before each photocatalytic run the MB-solution (70 ml) was equilibrated in the dark with the RR-TiO_2-Cu (35 g) for 30 min.

The light intensity reaching the photo-reactor was 90 mW cm^{-2} and was detected at the top of it. This light intensity was determined by a light dosimeter that measures the integrated photons in the Suntest simulator between 290 nm and 800 nm. The spectral range of photons generated by the Xe-lamp is shown In the Supplementary Fig. S5. The light in the Suntest cavity is reflected several times by the polished Al-walls.

Table 1
Weight percentage of TiO_2 and Cu in the RR samples of RR@TiO_2—Cu as determined by X-ray fluorescence (XRF).

Sample	%wt/% wt glass	
	TiO_2	Cu
RR@TiO_2	11.30	< 0.001
RR@TiO_2-Cu 0.004%	11.98	0.004
RR@TiO_2-Cu 0.018%	22.67	0.018
RR@TiO_2-Cu 0.053%	18.73	0.053
RR@TiO_2 - Cu 0.081%	13.04	0.081

2.2. ICP-MS determination of Ti-ions and Cu-ions leached out during MB discoloration

The determination by inductively coupled plasma mass-spectrometry (ICP-MS) of the Ti and Cu eluted during MB degradation was carried out by an ICP-MS Finnigan™ unit equipped with a double focusing reverse geometry mass spectrometer. It has an extremely low background signal and a high ion-transmission coefficient. The discoloured MB solution in contact with RR@TiO_2-Cu was digested with nitric acid 69% (1:1 $HNO_3 + H_2O$) to remove the organics in the solution and to insure that there were no adhered ions remaining on the flask wall. The samples droplets were introduced to the ICP-MS trough a peristaltic pump to the nebulizer chamber at ~7700 °C. This allows the complete sample evaporation. The Ti and Cu found in the nebulizer droplets were subsequently quantified by mass spectrometry (MS).

2.3. RR@TiO_2-Cu microstructure: surface properties

The atomic force spectroscopy (AFM) image signals were acquired in contact mode using a PSIA Xe-100 AFM. Silicon nitride cantilevers were used with feedback set points close to 1.0 nN. The AFM scanner and position sensors were calibrated using standard samples from Mikromash. The experimental error in the roughness was below 10%. The mean surface roughness (RMS) was calculated for scanned areas of 2 × 2 μM.

X-ray diffraction (XRD) of the RR@TiO_2-Cu Raschig rings were recorded on a Philips X'Pert PRO diffractometer equipped with an X'Celerator detector and a Ni-filtered Cu K radiation operating at 40 kV and 40 mA. The X-ray photoelectron spectroscopy (XPS) of the RR@TiO_2-Cu was carried out in an AXIS NOVA photoelectron spectrometer (Kratos Analytical, Manchester, UK) provided for with monochromatic AlK_a (hν=1486.6 eV) anode. The surface atomic concentration was determined from peak the XRD areas using the electrostatic correction according to Shirley [16–18]. The carbon C1 s at 284.6 eV was used as reference for the peak positions of Ti, C, and O the XPS spectrogram as well [16].

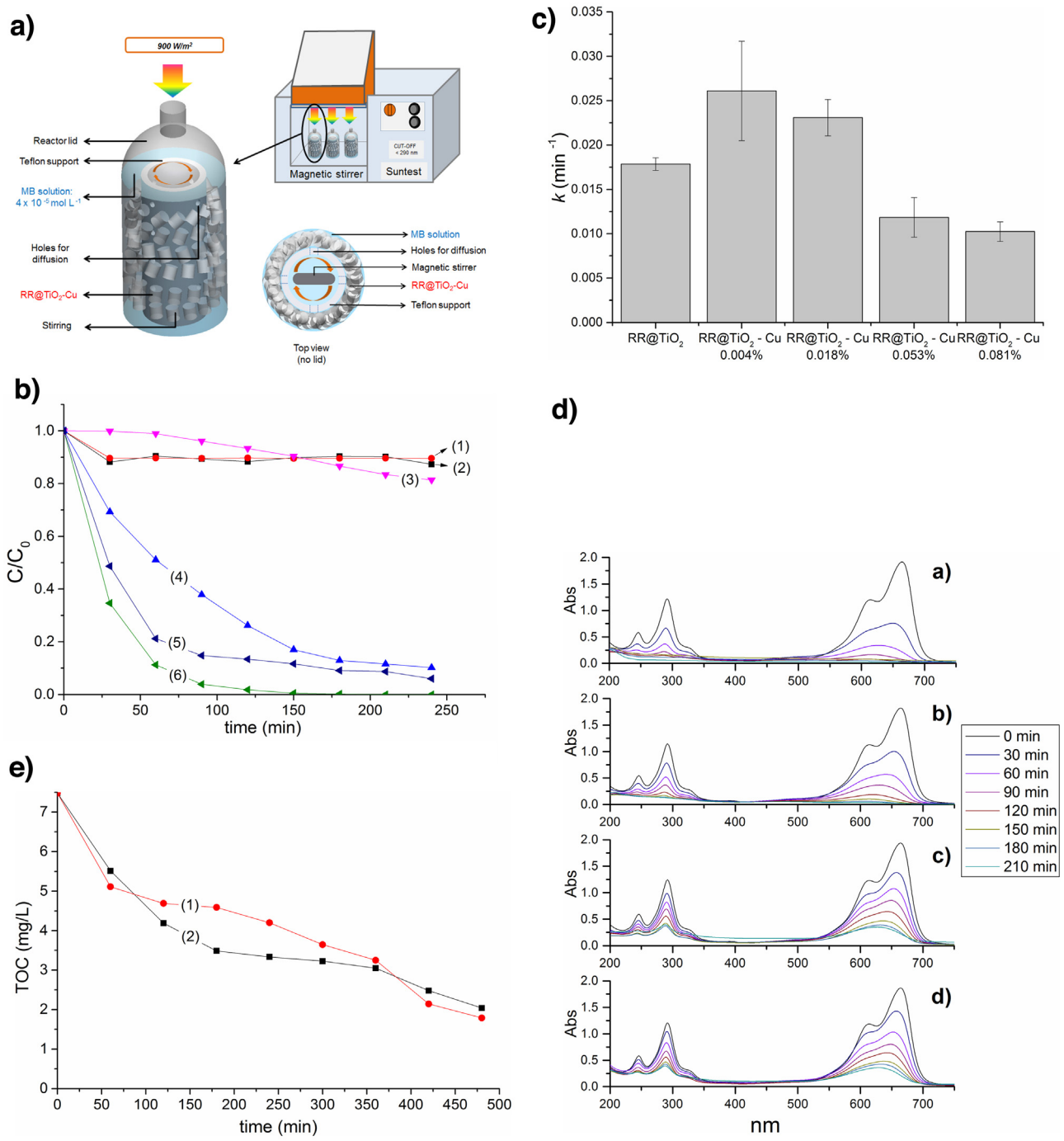

Fig. 1. (a) Schemes of the reactor and irradiation source. A Teflon support was placed concentrically inside the reactor for holding the RR@TiO_2—Cu bed. The reactors contained 70 ml of MB. Before photocatalytic reaction, the MB solution was equilibrated with the RR@TiO_2—Cu for 30 min (b) MB 4×10^{-5} mol L^{-1} solution discoloration under Suntest irradiation (90 mW cm^{-2}), Traces: (1) MB in contact with RR@TiO_2—Cu 0.004% in the dark, (2) MB in contact with Raschig rings in the dark, (3) MB in contact with Raschig rings under Suntest irradiation (90 mW cm^{-2}), (4) MB in contact with RR@TiO_2—Cu-0.053% under Suntest irradiation (90 W cm^{-2}), (5) MB in contact with RR@TiO_2 under Suntest irradiation (90 W cm^{-2}), (6) MB in contact with RR@TiO_2—Cu-0.004% under Suntest irradiation (90 W cm^{-2}). The initial pH of the solution was 5.7-6.0 (c) Dependence of the pseudo-first order rate constant k on the Cu-content of the RR@TiO_2—Cu photocatalyst during the discoloration of a solution MB 4×10^{-5} mol L^{-1} under Suntest light set at 90 m W cm^{-2}. The initial pH of the solution was 5.7-6.0. (d) Absorption spectra of MB 4×10^{-5} mol L^{-1} in contact with diverse RR@TiO_2—Cu photocatalysts under Suntest light set at 90 mW cm^{-2}: a) RR@TiO_2—Cu-0.004%, b) RR@TiO_2—Cu-0.018%, c) RR@TiO_2—Cu-0.053%, d) RR@TiO_2—Cu-0.081%. The initial pH of the solution was 5.7-6.0 (e) Total organic carbon (TOC) decrease during the photocatalytic degradation of MB 4×10^{-5} mol L^{-1} mediated by RR@TiO_2—Cu-0.004% under Suntest light (90 mW cm^{-2}). Initial pH of the MB solution: (1) pH 5.7 and (2) pH 10..

3. Results and discussion

3.1. MB discoloration kinetics

Table 1 presents the percentage of Cu and TiO_2 on the Raschig-rings obtained by X-ray fluorescence (XRF).

Fig. 1b, traces (1) and (2) show the MB adsorption in the dark on the RR@TiO_2-Cu 0.004% surface and on bare Raschig rings. There is no significant difference between runs (1) and (2) shown in Fig. 1b due to the low percentages of TiO_2 and Cu on the support (~15% TiO_2 and 0.004% Cu). Fig. 1b, trace (3) shows the low light effect on MB-discoloration in presence of Raschig rings during 240 min. A

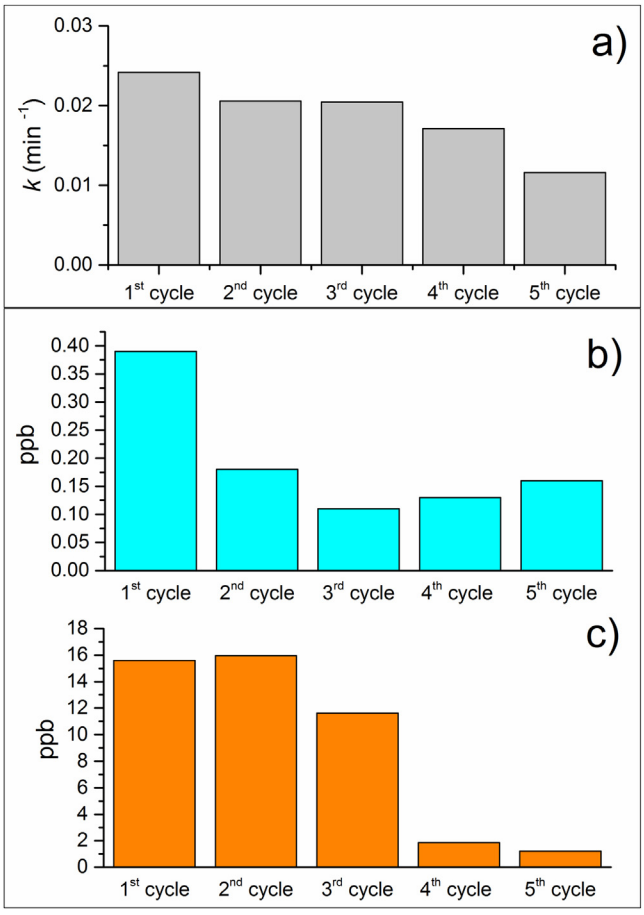

Fig. 2. (a) Rate constants (k) for the repetitive MB 4×10^{-5} mol L^{-1} discoloration by RR@TiO_2—Cu 0.004% 2b) Ti-ions released during MB-discoloration up to the 5th use cycle and (c) Cu-ions released during MB-discoloration up to the 5th use cycle. Suntest light set at 90 mW cm^{-2}.

RR@TiO_2-Cu-0.053% photocatalyst (trace (4)) shows no complete discoloration after 240 min. RR@TiO_2 is presented in trace (5), it displays a higher initial degradation rate compared to the RR@TiO_2-Cu-0.053% photocatalyst (trace (4)). RR@TiO_2-Cu-0.004% (trace (6)) is seen to lead to a faster discoloration compared to RR@TiO_2-Cu-0.053% (trace (4)) despite the lower Cu content (13.5 times less Cu). Also, RR@TiO_2-Cu-0.004% (trace (6)) performs better than RR@TiO_2 (trace (5) with higher initial degradation rate and being able to reach complete discoloration. These observations suggest that the Cu-sites deposited on the RR@TiO_2 surface may involve to intra-gap sites facilitating the TiO_2 charge transfer to MB under band-gap irradiation. However, at higher concentrations of Cu on the TiO_2 surface the Cu-sites may act as charge recombination centers decreasing the amount of photogenerated charges [1–6]. The position of the potential energy level of the Cu-intra-gap states lies between the TiO_2 vb (3.1 eV) and the TiO_2 cb (−0.1 eV) and can be estimated to be close to 0.15 eV [19]. The $Cu^{1+/2+}$ on the TiO_2 under band-gap irradiation would work as an electron acceptor enhancing MB-degradation [20].

Fig. 1c shows the pseudo-first order rate constant k of MB-discoloration as a function of the Cu-amount added to RR@TiO_2. Fig. 1c shows that the k for the MB-discoloration by RR@TiO_2-Cu-0.004% is higher compared to the k by the RR@TiO_2-Cu-0.018% photocatalyst and the other photocatalysts used to discolour MB (see Fig. 1c caption). This is the evidence for the RR@TiO_2-Cu-0.004% sample acting as a trap for the TiO_2vb (h+) increasing the charge separation and concomitantly decreasing the electron-hole recombination in TiO_2. Higher amounts of Cu decorating RR@TiO_2 above Cu 0.004% act as charge recombination sites/centers decreasing the k values during MB-discoloration (see Fig. 1c). The MB-discoloration kinetics as a function of the initial MB-concentration and the initial pH are reported in Supplementary material S2 & S3.

Fig. 1d presents the changes in the MB-absorbance spectra between 200 and 800 nm for MB solutions 4×10^{-5} mol L^{-1} in contact with RR@TiO_2 rings decorated with different amounts of Cu under Suntest light. The spectra in Fig. 1d (a–d) show that the MB-peak at 664 nm decreases more slowly as the Cu-content increases, which is consistent with results reported above in Fig. 1c. The MB-bands between 600 and 700 nm correspond to the conjugated π system comprising MB monomers/dimers [21]. The aromatic ring bands < 300 nm were observed also to disappear after around 120 min reflecting the progressive cleavage of the MB-aromatic ring. The small absorbance < 300 nm is assigned to long-lived organic intermediates left in solution [22]. The existence of long-lived intermediates in solution is further confirmed by the TOC results presented next for MB-discoloration/degradation in Fig. 1e.

Total organic carbon (TOC) decrease during the photocatalytic degradation of MB 4×10^{-5} mol L^{-1} mediated by RR@TiO_2-Cu-0.004% under Suntest light (90 mW cm^{-2}) at initial pH values of (1) pH 5.7 and (2) pH 10 is presented in Fig. 1e. For the two pH-values investigated the initial TOC drops by 75%. The mineralization varied only in a narrow range on the Cu amounts added on the RR@TiO_2 rings. This information is available in Supplementary material S4.

3.2. Repetitive MB-discoloration and evidence for the RR@TiO_2-Cu-0.004% stability

Fig. 2a shows the kinetic constants during the discoloration of MB by RR@TiO_2-Cu-0.004% up to the 5th use cycle. The k values vary only 10% up to the 3rd cycle and became lower in the 5th cycle. The photocatalyst rings were carefully washed and dried after each cycle. Fig. 2b shows by ICP-MS the Ti-ions leached after each recycling, the values reported in Fig. 2b were far below the allowed limit set by sanitary regulations for the toxicity on mammalian cells, up to one gram TiO_2/L [23]. Fig. 2c shows the ICP-MS amounts of the Cu-ions leached during the MB-discoloration into the solution. The values of 1 ppb of Cu detected after the 5th cycle were far below the limit of 25 ppb set by some sanitary regulations [24]. The low levels found for the release of Ti and Cu indicate that we are in the presence of an oligodynamic effect involving catalysis by contact with metal and/or oxides and taking place with an almost negligible release of ions [25].

3.3. Light intensity effects on the MB-discoloration kinetics and ROS detected during the MB-degradation

Fig. 3a shows the effect of light intensity on MB discoloration in the presence of RR@TiO_2—Cu. The faster MB-discoloration kinetics was observed under a higher applied light intensity increasing the photogenerated charges in TiO_2 making up > 99.9% of the RR@TiO_2-Cu 0.004%. The run shown in Fig. 3a, trace 4) at 90 mW cm^{-2}, was carried out in the presence of a cut-off filter 400 nm to block the UV light. Although the UV-light is present in a relation of about 1:20 compared to the photons in the Suntest simulated light cavity emitting light in the visible range (400–800 nm), their high energy is seen to contribute to the MB-discoloration up to ~50%. Only semiconductor materials show an increased amount of photo-generated charges due to a higher applied light intensity. Fig. 3a shows that TiO_2 and not the Cu intra-gap absorbers are responsible for the observed MB-discoloration. This suggests that the TiO_2cbe-

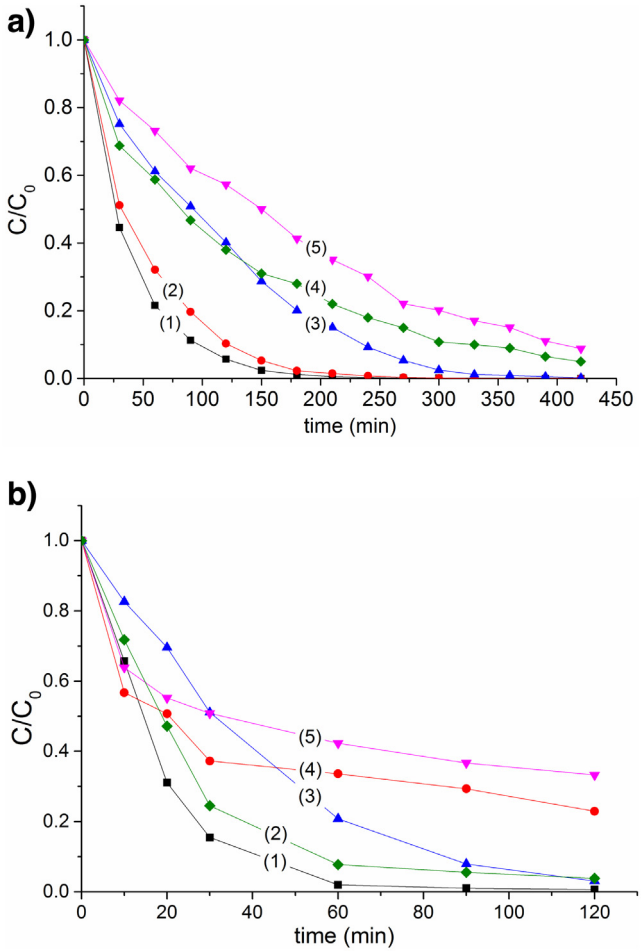

Fig. 3. (a) Discoloration of MB 4×10^{-5} mol L^{-1} on RR@TiO_2—Cu-0.004% as a function of the Suntest simulated sunlight intensity: (1) 120 mW cm^{-2}, (2) 90 mW cm^{-2}, (3) 60 mW cm^{-2}, (4) 90 mW cm^{-2} with UV filter at 400 nm and (5) 30 mW cm^{-1-2} (b) Discoloration of a solution MB (4×10^{-5} M) on RR@TiO_2—Cu 0.004% showing the intermediates radical-species being identified by appropriate scavengers: (1) run without scavengers, (2) run in the presence of 0.2 mM methanol, (3) run in the presence of 0.2 mM NaN_3, (4) run in the presence of 0.2 mM *p*-benzoquinone, (5) run in the presence of 0.2 mM EDTA-2Na.

reacting with the adsorbed O_2 is the main channel leading in later stages to MB-discoloration

Fig. 3b shows the scavenging of the intermediate radicals generated on the RR@TiO_2-Cu 0.004% surface: a) trace (2) MB-discoloration in the presence of methanol 20 mmol L^{-1} quenching the OH-radicals, b) trace (3) MB-discoloration in the presence of NaN_3 20 mmol L^{-1}, a scavenger of oxygen singlet $^1O_2$ [26,27], c) trace (4) MB-discoloration in the presence of benzoquinone 20 mmol L^{-1} [1,2] a quencher of $O_2^{\bullet -}/HO_2^{\bullet}$ [28,29], d) trace (5) MB-discoloration in the presence of 20 mmol L^{-1} ethylenediamine tetra-acetic acid disodium salt (EDTA-2Na), a widely used TiO_2vb (h^+) scavenger [1,6]. Trace (1) shows MB-discoloration without the addition of scavengers.

Results in Fig. 3b show that the scavenging follows the series: vb (h^+) > $O_2^{\bullet -}/HO_2^{\circ -}$ > $^1O_2$ > $OH^{\bullet}$. The dissolved O_2 (8 mgL^{-1}) is not only a TiO_2 electron scavenger but its presence is necessary to generate the $HO_2^{\circ -}$. At pH > 4.8, more than 50% of the $HO_2^{\circ -}$ is present in the form of $O_2^{\bullet -}$. This form of the HO_2^{o-} radical predominates, since the initial pH of the MB-solution was ~6.0 decreasing during the MB-discoloration to a value of 4.7. The OH°-radicals scavenged by methanol in Fig. 3b, trace 2) imply one electron reduction OH°/OH^{--} with E_0 1.90 V NHE and show a smaller scavenging effect compared to O_2^{-}/HO_2° with a lower potential of E_0 0.75 V NHE. The lifetime and concentration of the OH°-radicals is much lower compared to the less energetic O_2^{-}/HO_2^{-o} [30].

Azide NaN_3 has been generally reported as a singlet $^1O_2$ scavenger [1,2]. However, it also reacts with OH-radicals with a similar rate as it does with singlet $^1O_2$ [3,15]. For this reason, the data reported in Fig. 3b wouldn't indicate in a specific way the effect of the singlet oxygen during MB-discoloration. Another issue to consider is that the CuOcbe$^-$ could react in two ways: a) directly with O_2 leading to $O_2^{\bullet -}$ or b) reducing the CuO to Cu^+, as noted in Eqs. (1) and (2) below:

$$CuO(cbe^-) + O_2 \rightarrow CuO + O_2^{\bullet -} \quad (1)$$

$$CuO(cbe^-) \rightarrow CuO(Cu^+) \quad (2)$$

Reaction (2) is much faster than the CuO dissolution [19,20], shown in Eq. (3). The reaction (Eq (3)) involves CuO(Cu^+) and could possibly lead to the reaction of CuO with the holes TiO_2vbh+.

$$CuO(Cu^+) \rightarrow CuO\ \text{vacancy} + Cu^+ \quad (3)$$

EDTA is used generally as a hole scavenger in TiO_2 photocatalysis. But it may not play this role in the case of CuO mediated photocatalysis. We observed that by scavenging TiO_2vbh+ with EDTA, the MB became colorless. After contacting the MB-solution with fresh air (O_2), the solution became blue again. This suggests that while blocking the TiO_2vbh+, MB gets reduced to the leuco form of methylene blue (LMB).

Based on these findings, the design of a reactor with a RR@TiO_2-Cu photocatalyst may consider two factors: a) good contact between the photocatalyst and the solution and b) good mixing inside the reactor for oxygen diffusion, which will improve the oxygenated radicals' formation.

3.4. Suggested reaction mechanism, involvement of Cu intra-gap states

Metals/oxides have been shown to increase the charge separation on semiconductors [1,6,19] leading to new interfaces. The discoloration mechanism is suggested to proceed initially by the photogenerated TiO_2 electrons transferred to the TiO_2cb by the Cu intra-gap states in the TiO_2 as suggested in Fig. 4.

$$TiO_2\text{—}Cu + h\nu \rightarrow \text{vb}\ (h^+) + \text{cb}\ (e\text{-}) \quad (4)$$

The direct photosensitization of MB in the presence of RR@TiO_2—Cu under Suntest simulated sunlight shown in Fig. 4 may be suggested as:

$$MB + [RR@TiO_2\text{—}Cu] + h\nu \rightarrow [MB^{*}\cdots RR@TiO_2\text{—}Cu] \rightarrow MB^{+\bullet} + [RR@TiO_2\text{—}Cu] + \text{cb}(e\text{-}) \quad (5)$$

Under sunlight irradiation, both the MB and TiO_2 are photosensitized, MB injects electrons into the TiO_2cb and in parallel converts MB to the MB^{+*} cation radical. The electron injected by the MB into the TiO_2 reacts with O_2 and generates highly oxidative radicals leading to the discoloration/degradation of MB as shown in Fig. 4 [20]. The low laying Cu intra-gap states promote the indirect transition of the electron from TiO_2 vb (h^+) to the TiO_2cb. This is consistent with the results reported in Fig. 1b for RR@TiO_2—Cu 0.004% photocatalyst. The $Cu^{1+/2+}$ intra-gap states also interact with the RR@TiO_2—Cu 0.004% adsorbed O_2. In this way, the recombination rate of the TiO_2 e-/h+ pairs is hindered improving the photocatalyst MB-degradation. The addition of

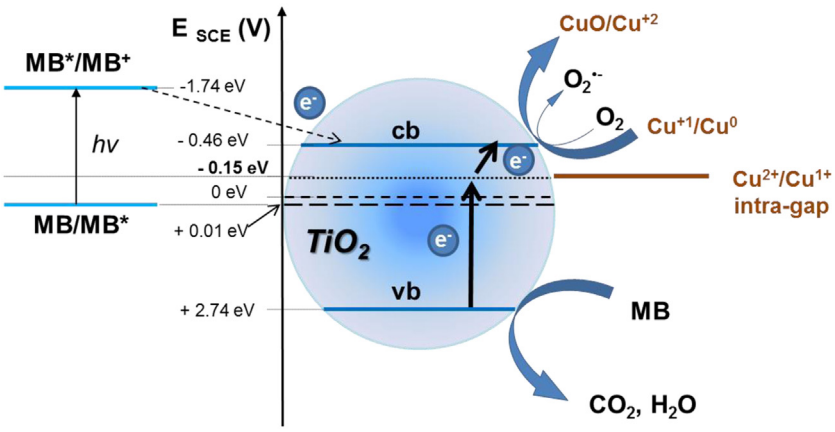

Fig. 4. Suggested scheme for RR@TiO_2—Cu intra-gap mediated electron transition under sunlight irradiation leading to MB-discoloration/degradation. For further details see text.

Cu > 0.004% makes the Cu-act as a recombination center because the thickness of the space layers decreases with increasing Cu-content [19]. The Cu^{1+} would also reduce the air (O_2) consuming electrons or re-oxidize to Cu-ions by the photogenerated TiO_2 holes to Cu^{2+} [20,31,32].

The $Cu^{1+/2+}$ and Ti^{3+} intermediate donor levels may be present due to the back charge transfer reaction: e- $+Ti^{4+} \rightarrow Ti^{3+}$ following the reaction stated above in Eq. (4) [33]. The vb(h+) reacts with the TiO_2 O-vacancies formed concomitant to the Ti^{3+} trough the channel: $h^+ + O^{2-} \rightarrow O^-$ leading subsequently to the re-population of Cu^{1+} in the $Cu^{1+/2+}$ intra-gap states. Sputtered Cu-polystyrene was reported to present initially predominantly Cu^{1+} states followed in later reaction stages by Cu^{2+} [15]. Cu intra-gap sates in a TiO_2/Cu sputtered catalyst surface were reported to lead to more OH^{oo}-radicals, due to additional vb (h+) [16]. As long as the RR@TiO_2-Cu 0.004% in Fig. 4 is photoactivated by light, it will continuously produce cbe- reacting with O_2 leading to the formation of oxidative intermediate radicals.

3.5. Surface properties of RR@TiO_2-Cu

3.5.1. Diffuse reflectance spectroscopy (DRS)

Fig. 5 shows the DRS spectra of the samples in Kubelka-Munk units. Cu is seen to move the RR@TiO_2 absorption drastically into the visible region. Similar optical modifications were found by Kapilashrami et al. [34] when doping TiO_2 with non-metals. Trace (1) shows the DRS spectrum of TiO_2 Degussa P-25 on glass. The Cu^{2+} ionic-radii are larger than the one of Ti^{4+}, and therefore it would be difficult for the Cu^{2+} to replace Ti^{4+} in the crystal lattice [33,35]. The Cu-species may decorate the surface of the TiO_2 matrix. If Cu cations would be incorporated in the TiO_2 lattice by substituting Ti^{4+}, the electro-neutrality demand would require the additional formation of O-vacancies. Peaks between 320 and 440 nm in Fig. 5, traces 2, 3 have been attributed to $(Cu–O—Cu)^{2+}$ clusters in highly dispersed states. The peaks between 400 and 500 nm (Fig. 5, traces 4, 5) were assigned to three dimensional Cu^{1+} clusters in CuO [36,37].

3.5.2. X-ray diffraction (XRD)

The XRD-spectrograms in Fig. 6 are shown for RR@TiO_2-Cu 0.018% in trace (1) and for RR@TiO2-Cu 0.053% in trace (2). The presence of TiO_2 Degussa P-25 is confirmed by the peaks at 25° and 27.5° for anatase and rutile respectively, as reported by Hanaor et al. [38]. The size of the anatase crystals was assessed based on the (101) reflection in the spectra (1) and (2) and the calculations lead to particle size of ~20 nm in both cases. The calculations were made by means of the Debye-Scherrer equation, noted in Eq. (6).

$$D = \frac{k\lambda}{\beta cos\theta} \quad (6)$$

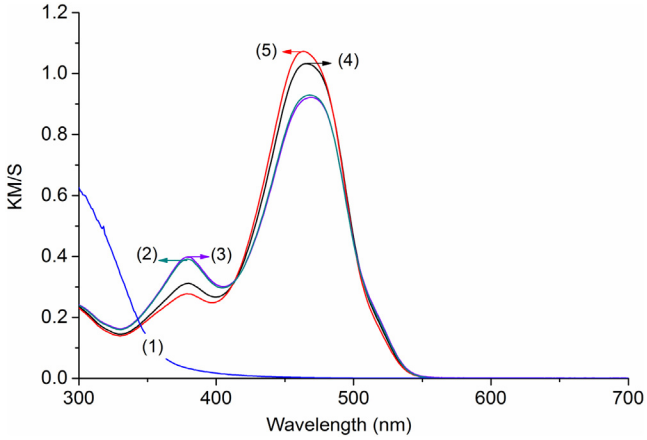

Fig. 5. DRS spectra for different Cu weight percentages in RR@TiO_2. (1) RR@TiO_2, (2) RR@TiO_2—Cu 0.004%, (3) RR@TiO_2—Cu 0.018%, (4) RR@TiO_2—Cu 0.053% and (5) RR@TiO_2—Cu 0.081%.

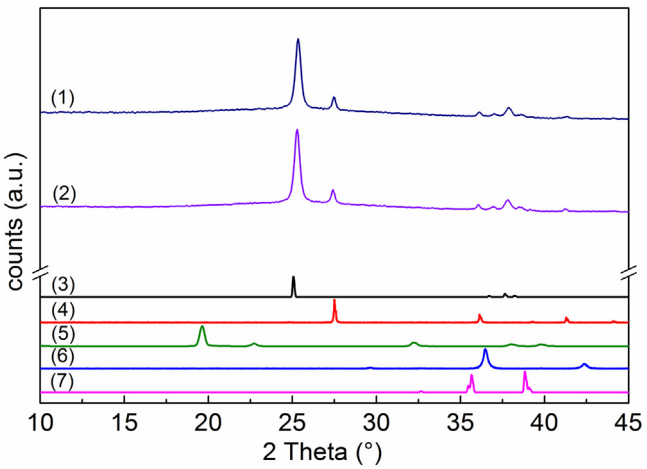

Fig. 6. XRD for different Cu weight percentages in RR@TiO_2 and references of TiO_2, Cu and Cu oxides. (1) RR@TiO_2 – Cu 0.018%, (2) RR@TiO_2 – Cu 0.053%. Reference XRD: (3) Anatase (R100013), (4) Rutile (R040049), (5) Copper (R061078), (6) Cu_2O (R050384), (7) CuO (R120076) [42].

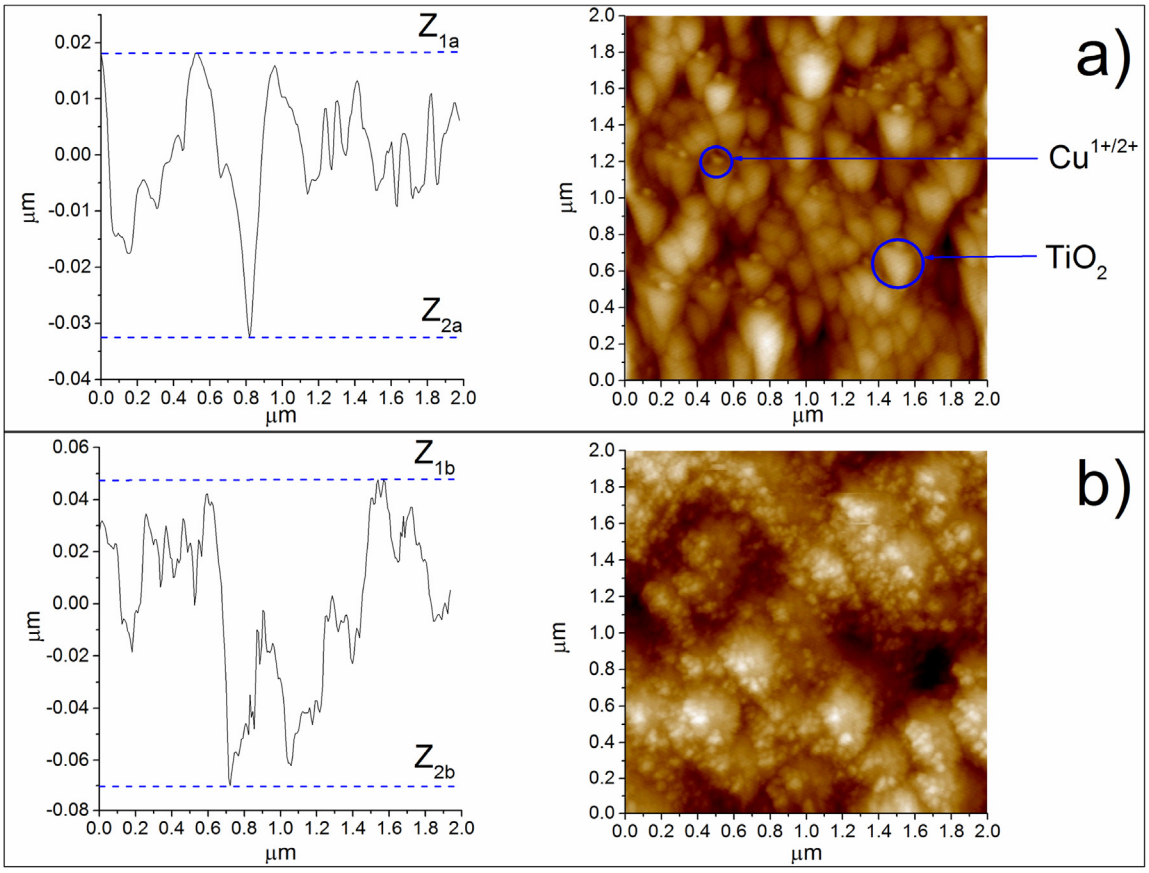

Fig. 7. (a) AFM- topography of RR@TiO_2—Cu 0.018% taken at a resolution of (2 × 2 μM), (b) AFM-topography of RR@TiO_2—Cu 0.081% taken at a resolution of (2 × 2 μM).

For Eq. (6), D stands for the crystal size in nm, κ = as the shape factor which is usually fixed as 0.89, λ = as the wavelength which is taken as 0.154 nm, β = which is the full width at half maximum for the prominent peak, and θ = as the Bragg's diffraction angle in radians [39,40]. The characteristic peaks of Cu and Cu oxides between 35° and 40° in Fig. 6, traces (1) and (2) appear as overlapping peaks of anatase (trace (3)), Cu (trace (5)), Cu_2O (trace (6)) and CuO (trace (7)). Cu-oxides peaks were found by XRD for higher Cu doping percentages (> 5%) by Bensouici et al., [41]. The Cu and Cu-oxide peaks in Fig. 6 are referenced to the RRUFF database [42]; they appear between 35° and 40° for Cu, Cu_2O and CuO. In the course of this study, we could not sort out the different Cu-oxide species due to the extremely low amounts of Cu deposited on the catalyst surface.

3.5.3. Atomic force microscopy (AFM) and roughness (Rg)

Fig. 7 shows AFM-topography images of RR@TiO_2-Cu 0.018% (a) and RR@TiO_2-Cu 0.081% (b) for two scanning areas of 2 × 2 μM. The topography of RR@TiO_2-Cu 0.004% sample is not presented because the low amount of Cu could not be detected; only TiO_2 aggregates presented adequate signals. Fig. 7a) shows TiO_2 and Cu-agglomerates of ∼200 nm ∼20 nm in size respectively. The RR@TiO_2-Cu 0.018% samples presents a roughness (Rg) ≅ 11.8 nm. In this case, the topography of the AFM *contour* in Fig. 7a) shows peaks relatively closely packed to each other providing the contact points with MB [43]. Fig. 7b) illustrates the TiO_2-Cu 0.081% sample. TiO_2 and Cu agglomerates of ∼200 nm and ∼20 nm in size respectively were observed. The RR@TiO_2-Cu 0.081% sample presents roughness (Rg) ≅ 23.9 nm. The topography of the AFM *contour* in Fig. 7b) shows deeper and wider valleys to accommodate the MB dye providing less surface contact between the photocatalyst and MB.

3.5.4. X-Ray photoelectron spectroscopy (XPS)

Fig. 8 and Table 2 show the peak variation and the surface percentage atomic concentration of the elements present in the RR@TiO_2-Cu 0.004% during discoloration/degradation of the MB diluted solution. The XPS signal at time zero was taken after the sample was contacted with the MB solution for 30 min in the dark. Fig. 8a) shows the Ti2p doublet shift from 456.98 eV to 457.15 eV. This provides the evidence for a redox reaction occurring during the MB-degradation involving Ti^{3+}/Ti^{4+}. The appearance of Ti^{3+} species is associated to the peak initial peak shift of Ti^{4+} >0.2 eV [3]. Redox behavior was also observed for $Cu2p_{3/2}$ and O1 s since peak shifts from 930.68 eV to 931.08 eV and from 528.19 to 528.39 were observed for both elements respectively as shown in Fig. 8b) and Fig. 8c) [17,18]. Fig. 8d) shows the XPS C1 s at time zero. It displays the contribution of several carbon bonds like C—C, C=C, COH, C=O, C—H etc., found in the MB such as C—C (sp^2), C—C (sp^3), C—N-R2 [44]. The XPS carbon peaks after 120 min irradiation (trace (2) in Fig. 8d)) were less intense, meaning a decrease in atomic carbon, consistent with the values for C1 s reported in Table 2, due to changes in the C—C (sp^2) and C—C (sp^3) during the MB degradation.

In Table 2 the percentage of C1 s is seen to decrease within 120 min due to MB discoloration, but a strong residual C1 s is noticed after 120 min. This observation is consistent with the TOC-results reported in Fig. 1d. No N-species adsorbed on the photocatalyst surface were detected by XPS as shown In Table 2 by the low atomic percentages found for N. The small amounts of

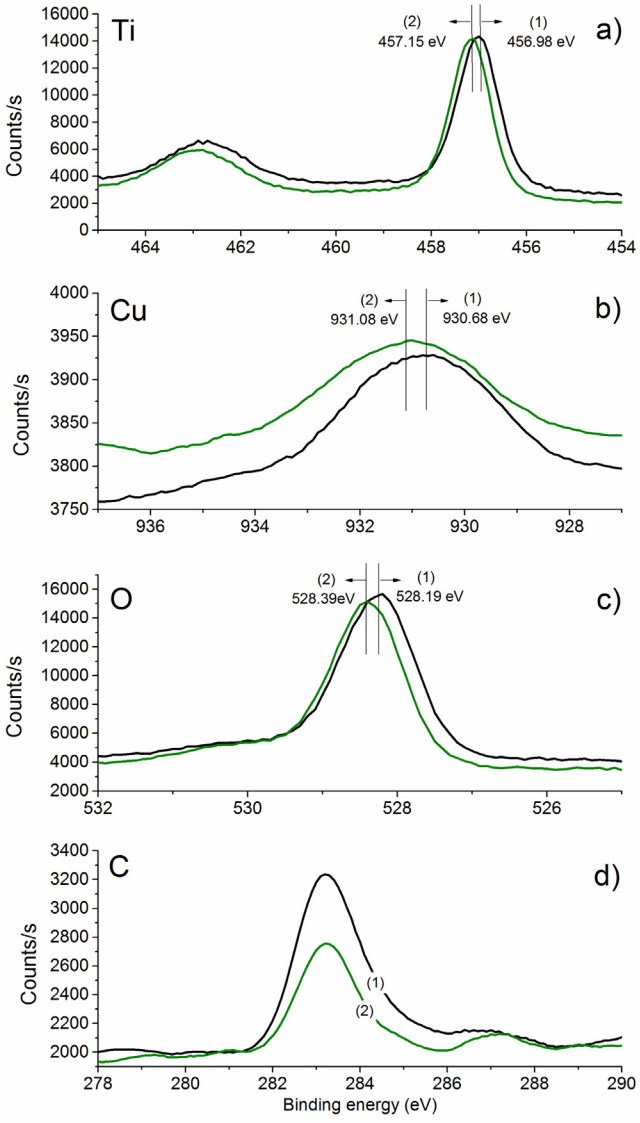

Fig. 8. XPS signals of Ti (a), Cu (b), O (c) and C (d) at time zero (1) and after discoloration of a MB 4×10^{-5} mol L^{-1} solution on RR@TiO_2–Cu 0.004% (2). Suntest irradiation set at 90 mW cm^{-2}.

S- remained constant in experimental error during the MB-degradation. A complicated pattern is noticed for the percentage variation of O1 s signals as a function of time reported in Table 2. This may be due to the complicated nature of the O-containing intermediate radicals generated during the MB-degradation. The percentage of Cu could not be reported in the last column of Table 2 due to the low amounts of Cu in the RR@TiO_2-Cu 0.004% sample.

Table 2
Atomic percentage concentration of the elements of the sample RR@TiO_2—Cu-0.004%, during the degradation of MB: 4×10^{-5} mol L^{-1}.

Irradiation time (min)	C1s	N1s	O1s	S2p	Ti2p	Cu2$p_{3/2}$
0	18.04	3.54	62.48	0.18	24.06	0
30	16.72	1.40	76.03	0.58	20.23	0
60	13.51	0.44	70.22	0.52	22.30	0
120	13.11	0.40	60.42	0.37	23.72	0

4. Conclusions

Cu-decoration seems to induce an intra-gap-electronic state in the TiO_2 facilitating the indirect electron transition in the TiO_2 band-gap and leading to an accelerated MB-degradation kinetics. The results obtained during MB discoloration showed that a Cu-addition of 0.004% on RR@TiO_2 led to the highest photocatalytic activity. The addition of Cu on RR@TiO_2 shifts strongly the photocatalyst absorbance into the visible region. The Cu intra-gap states in RR@TiO_2-Cu could not be characterized due to the low amounts of Cu present in the photocatalyst. Higher Cu-levels on the TiO_2 surface seem to act as recombination centers for the photogenerated charges decreasing the rate of MB-discoloration. By the use of appropriate scavengers (TiO_2vb (h +) was found to be the most important intermediate species leading to MB-degradation. The XPS-shifts during the photocatalytic degradation of MB provides the evidence for redox events between CuOx/TiO_2 and the MB. The AFM results indicate that a low Cu-loading on the RR@TiO_2 rings showed a close packed *contour* compared to the wide-spaced *contour* obtained with higher Cu-loadings. A close packed *contour* in the low Cu-loading provides more contact points with MB leading to faster degradation.

Acknowledgments

We thank the EPFL and the EC7th Limpid FP project (Grant No. 3101177) for financial support. We also thank Stefanos Giannakis, Sami Rtimi (EPFL) and Paola Villegas (Universidad de Antioquia, Colombia) for the valuable discussions during the course of this work.

Appendix A. Supplementary data

Supplementary data associated with this article can be found, in the online version, at http://dx.doi.org/10.1016/j.jece.2016.12.006.

References

[1] A. Fujishima, X. Zhang, D.A. Tryk, TiO_2 photocatalysis and related surface phenomena, Surf. Sci. Rep. 63 (2008) 515–582.
[2] M. Pelaez, N.T. Nolan, S.C. Pillai, M.K. Seery, P. Falaras, A.G. Kontos, P.S.M. Dunlop, J.W.J. Hamilton, J.A. Byrne, K. O'Shea, M.H. Entezari, D.D. Dionysiou, A review on the visible light active titanium dioxide photocatalysts for environmental applications, Appl. Catal. B: Environ. 125 (2012) 331–349.
[3] S. Banerjee, S.C. Pillai, P. Falaras, K.E. O'Shea, J.A. Byrne, D.D. Dionysiou, New insights into the mechanism of visible light photocatalysis, J. Phys. Chem. Lett. 5 (2014) 2543–2554.
[4] V. Etacheri, C. Di Valentin, J. Schneider, D. Bahnemann, S.C. Pillai, Visible-light activation of TiO_2 photocatalysts: advances in theory and experiments, J. Photoch. Photobio. C 25 (2015) 1–29.
[5] J. Schneider, M. Matsuoka, M. Takeuchi, J.L. Zhang, Y. Horiuchi, M. Anpo, D.W. Bahnemann, Understanding TiO2 photocatalysis: mechanisms and materials, Chem. Rev. 114 (2014) 9919–9986.
[6] C. Pulgarin, J. Kiwi, Overview on photocatalytic and electrocatalytic pretreatment of industrial non-biodegradable pollutants and pesticides, Chimia 50 (1996) 50–55.
[7] M.J. Sampaio, C.G. Silva, A.M.T. Silva, V.J.P. Vilar, R.A.R. Boaventura, J.L. Faria, Photocatalytic activity of TiO_2-coated glass raschig rings on the degradation of phenolic derivatives under simulated solar light irradiation, Chem. Eng. J. 224 (2013) 32–38.
[8] S. Sabar, M.A. Nawi, W.S.W. Ngah, Photocatalytic removal of Reactive Red 4 dye by immobilised layer-by-layer TiO_2/cross-linked chitosan derivatives system, Desalin. Water Treat. 57 (2016) 5851–5857.
[9] J. Saien, M. Asgari, A.R. Soleymani, N. Taghavinia, Photocatalytic decomposition of direct red 16 and kinetics analysis in a conic body packed bed reactor with nanostructure titania coated Raschig rings, Chem. Eng. J. 151 (2009) 295–301.
[10] A.L. Linsebigler, G.Q. Lu, J.T. Yates, Photocatalysis on TiO_2 surfaces – principles, mechanisms, and selected results, Chem. Rev. 95 (1995) 735–758.
[11] P. Raja, M. Bensimon, A. Kulik, R. Foschia, D. Laub, P. Albers, R. Renganathan, J. Kiwi, Dynamics and characterization of an innovative Raschig rings-TiO_2 composite photocatalyst, J. Mol. Catal. A-Chem. 237 (2005) 215–223.

[12] P. Raja, V. Nadtochenko, U. Klehm, J. Kiwi, Structure and performance of a novel TiO_2-phosphonate composite photocatalyst, Appl. Catal. B-Environ. 81 (2008) 258–266.
[13] P. Raja, J. Bandara, P. Giordano, J. Kiwi, Innovative supported composite photocatalyst for the oxidation of phenolic waters in reactor processes, Ind. Eng. Chem. Res. 44 (2005) 8959–8967.
[14] A. Mills, S. Le Hunte, An overview of semiconductor photocatalysis, J. Photochem. Photobiol. A: Chem. 108 (1997) 1–35.
[15] A. Mills, J.S. Wang, Photobleaching of methylene blue sensitised by TiO_2: an ambiguous system? J. Photoch. Photobio. A 127 (1999) 123–134.
[16] D. Briggs, W.M. Wanger, L.E. Riggs, J.F. Moulder, G.E. Muilenberg, Handbook of X-ray Photoelectron Spectroscopy, Vol 3, Perkin-Elmer Corp., Physical Electronics Division, Eden Prairie, Minnesota, USA, 1979.
[17] J. Nogier, M. Delamar, P. Ruiz, B. Delmon, J.P. Bonnelle, M. Guelton, L. Gengembre, J.C. Vedrine, M. Brun, P. Albers, K. Seibold, M. Baerns, H. Papp, J. Stoch, L.T. Andersson, J. Kiwi, R. Thampi, M. Gratzel, G.C. Bond, N. Verma, J.C. Vickerman, R.H. West, X-Ray photoelectron-Spectroscopy of TiO_2/V_2O_5 catalysts, Catal. Today 20 (1994) 109–123.
[18] D.A. Shirley, High-resolution X-Ray photoemission spectrum of the valence bands of gold, Phys. Rev. B 5 (1972) 4709–4714.
[19] A.J. Nozik, Photoelectrochemistry – applications to solar-Energy conversion, Annu. Rev. Phys. Chem. 29 (1978) 189–222.
[20] S. Rtimi, C. Pulgarin, R. Sanjines, J. Kiwi, Accelerated self-cleaning by Cu promoted semiconductor binary-oxides under low intensity sunlight irradiation, Appl. Catal. B: Environ. 180 (2016) 648–655.
[21] J. Tang, Z. Zou, J. Yin, J. Ye, Photocatalytic degradation of methylene blue on $CaIn_2O_4$ under visible light irradiation, Chem. Phys. Lett. 382 (2003) 175–179.
[22] B. Roig, C. Gonzalez, O. Thomas, Monitoring of phenol photodegradation by ultraviolet spectroscopy, Spectrochim. Acta A 59 (2003) 303–307.
[23] E. Rentz Do Comm Cnmo, Viral pathogens and severe acute respiratory syndrome: oligodynamic Ag+ for direct immune intervention, J. Nutr. Environ. Med. 13 (2003) 109–118.
[24] H.A. Jeng, J. Swanson, Toxicity of metal oxide nanoparticles in mammalian cells, J. Environ. Sci. Heal A 41 (2006) 2699–2711.
[25] W.K. Nägeli, Neue denkschr. allgemein. schweiz. gesellsch. ges. naturweiss. 1893, bd XXXIII abt 1, english archive: Nägeli, Denkschr. Allgemein. Naturfor. Ges. 33 (1893) 174–182.
[26] L. Suárez, C. Pulgarin, C. Roussel, J. Kiwi, Preparation kinetics, mechanism and properties of semi-transparent photocatalytic stable films active in dye degradation, Appl. Catal. A: Gen. 516 (2016) 70–80.
[27] K. Vinodgopal, P.V. Kamat, Photochemistry of textile azo dyes – spectral characterization of excited-State, reduced and oxidized forms of acid orange-7, J. Photoch. Photobio. A 83 (1994) 141–146.
[28] P. Piccinini, C. Minero, M. Vincenti, E. Pelizzetti, Photocatalytic interconversion of nitrogen-containing benzene derivatives, J. Chem. Soc. Faraday T. 93 (1997) 1993–2000.
[29] K.B. Patel, R.L. Willson, Semiquinone free radicals and oxygen. Pulse radiolysis study of one electron transfer equilibria, Journal of the Chemical Society, Faraday Trans. 1: Phys. Chem. Condens. Phases 69 (1973) 814–825.
[30] P. Wardman, Reduction potentials of one-electron couples involving free-radicals in aqueous-solution, J. Phys. Chem. Ref. Data 18 (1989) 1637–1755.
[31] X.Q. Qiu, M. Miyauchi, K. Sunada, M. Minoshima, M. Liu, Y. Lu, D. Li, Y. Shimodaira, Y. Hosogi, Y. Kuroda, K. Hashimoto, Hybrid CuxO/TiO_2 nanocomposites As risk-Reduction materials in indoor environments, Acs Nano 6 (2012) 1609–1618.
[32] L.G. Devi, R. Kavitha, A review on non metal ion doped titania for the photocatalytic degradation of organic pollutants under UV/solar light: role of photogenerated charge carrier dynamics in enhancing the activity, Appl. Catal. B-Environ. 140 (2013) 559–587.
[33] R.D. Shannon, Revised effective ionic-Radii and systematic studies of interatomic distances in halides and chalcogenides, Acta Crystallogr. A 32 (1976) 751–767.
[34] M. Kapilashrami, Y. Zhang, Y.-S. Liu, A. Hagfeldt, J. Guo, Probing the optical property and electronic structure of TiO2 nanomaterials for renewable energy applications, Chem. Rev. 114 (2014) 9662–9707.
[35] L. Yu, S. Yuan, L.Y. Shi, Y. Zhao, J.H. Fang, Synthesis of Cu^{2+} doped mesoporous titania and investigation of its photocatalytic ability under visible light, Micropor. Mesopor. Mater. 134 (2010) 108–114.
[36] G. Colón, M. Maicu, M.C. Hidalgo, J.A. Navío, Cu-doped TiO2 systems with improved photocatalytic activity, Appl. Catal. B: Environ. 67 (2006) 41–51.
[37] H. Praliaud, S. Mikhailenko, Z. Chajar, M. Primet, Surface and bulk properties of Cu-ZSM-5 and Cu/Al_2O_3 solids during redox treatments. Correlation with the selective reduction of nitric oxide by hydrocarbons, Appl. Catal. B-Environ. 16 (1998) 359–374.
[38] D.A.H. Hanaor, C.C. Sorrell, Review of the anatase to rutile phase transformation, J. Mater. Sci. 46 (2011) 855–874.
[39] B.D. Cullity, Elements of X-ray Diffraction, Addison-Wesley Pub. Co., Reading, Mass, 1956.
[40] P. Harold Klug, E. Leroy Alexander, X-ray Diffraction Procedures for Polycrystalline and Amorphous Materials, Wiley, New York, 1974.
[41] F. Bensouici, M. Bououdina, A.A. Dakhel, R. Tala-Ighil, M. Tounane, A. Iratni, T. Souier, S. Liu, W. Cai, Optical, structural and photocatalysis properties of Cu-doped TiO_2 thin films, Appl. Surf. Sci. 395 (2017) 110–116.
[42] RRUFF project, Department of Geosciences, University of Arizona. http://rruff.info/, 2016, (accessed 08 August2016).
[43] O. Seddiki, C. Harnagea, L. Levesque, D. Mantovani, F. Rosei, Evidence of antibacterial activity on titanium surfaces through nanotextures, Appl. Surf. Sci. 308 (2014) 275–284.
[44] I. Uvarova, Nanostructured materials in medicine. State of the art in Ukraine, Nato. Sci. Ser. Ii. Math. 102 (2003) 1–13.